PNAS RESEARCH ARTICLE | EARTH, ATMOSPHERIC, AND PLANETARY SCIENCES OPEN ACCESS

North Atlantic and the Barents Sea variability contribute to the 2023 extreme fire season in Canada

Guanyu Liu[a], Jing Li[a,1], Xichen Li[b], and Tong Ying[a]

Affiliations are included on p. 8.

Edited by Venkatachalam Ramaswamy, National Oceanic and Atmospheric Administration Geophysical Fluid Dynamics Laboratory, Princeton, NJ; received July 27, 2024; accepted October 2, 2024 by Editorial Board Member Robert E. Dickinson

In the late spring to summer season of 2023, Canada witnessed unprecedented wildfires, with an extensive burning area and smoke spreading as far as the East Coast of the United States and Europe. Here, using multisource data analysis and climate model simulations, we show that an abnormally warm North Atlantic, as well as an abnormally low Barents Sea ice concentration (SIC), are likely key climate drivers of this Canadian fire season, contributing to ~80% of the fire weather anomaly over Canada from June to August 2023. Specifically, the warm North Atlantic forms an anomalous regional zonal cell with ascending air over the Atlantic and descending air encircling Canada, creating hot and dry local conditions. Meanwhile, reduced Barents SIC leads to a high-pressure center and reinforces the dry northern winds in Canada through Rossby wave dynamics. These exacerbated dry and hot conditions create a favorable environment for the ignition and spread of fires, thus contributing to the prolonged and extreme fire season in Canada. These teleconnections can extend to decadal scales and have important implications for understanding and predicting decadal fire activity in Canada and the surrounding regions.

extreme fire | Canada | nature variability | teleconnection | contribution

Significance

The 2023 Canadian fire season witnessed an unprecedented extremity. However, the underlying causes remain elusive. Our study reveals that warmer North Atlantic waters and reduced Barents Sea ice concentration might be crucial contributing factors, accounting for 80% of the fire weather anomaly. The warmth in the North Atlantic gives rise to a regional zonal cell, while the diminished ice strengthens the dry southward winds. To the best of our knowledge, this is the inaugural study to identify these climate drivers for the 2023 Canadian fire season, and it underlines the imperative for policymakers to confront the challenges presented by climate change. Our research also holds implications for comprehending and forecasting fire activity in Canada and other high-risk regions.

Wildfires serve as pivotal natural disturbance agents, exerting profound effects on biogeochemical cycles, ecosystem structures, and hydrological dynamics in various ecological system (1). Canada, renowned for its extensive forest coverage and diverse array of tree species, has experienced substantial wildfire occurrences resulting from both human activities and lightning strikes (2, 3). This region has witnessed a notable increase in fires of both natural and anthropogenic origins in boreal spring and autumn, with the most catastrophic wildfire season on record observed in late spring to summer in 2023. As of the end of 2023, the cumulative land area devastated by wildfires in Canada has exceeded seven times the annual average and double the previous maximum in 1989 (4), emitting more than doubled Canada's planned cumulative anthropogenic emissions reductions in 10 y (4, 5). Moreover, the smoke associated with the burning has traveled as far as Eastern United States or even Europe, exerting serious impact on the ecosystems, public health, and biological communities globally (5). Additionally, there are indications that certain regions of Canada have witnessed an increase in area burned, the number of fires, seasonal fire severity, extreme weather events, and fire season durations in recent decades (4–8). Against the backdrop of climate change and other anthropogenic influences on forests and fire regimes, wildfires in Canada have become a major climate and environmental concern (9–11). Therefore, it is essential to understand the underlying mechanisms that contribute to these fires, especially those associated with climate variability.

Wildfires are mainly triggered by abnormal weather conditions, especially droughts and heatwaves (8). These extreme weather events are caused by a combination of factors including ocean circulation patterns, positive geopotential height anomalies, and climate change. The above factors interact both spatially and temporally to increase fuel flammability, which in turn affects Canada's fire activity indirectly (12). Similarly, the unprecedented burning season of 2023 in Canada is also believed to be associated with abnormal weather conditions, including high temperatures, low precipitation, and stronger northerly winds. These conditions are formed through a complicated interaction between remote forcing and local processes (5). While global warming increases the likelihood of these extreme events (13–15), the particular climate variability that causes the abnormally high fire-prone weather conditions in the late spring to summer season of 2023 in Canada remains unclear.

Canadian weather can be influenced by both local and remote climate variability. In particular, ocean variability, such as those of North Atlantic, the Arctic, and Pacific (16–19), can remarkably impact Canadian climate through atmospheric teleconnection mechanisms. For example, statistical analyses have also presented compelling evidence on the role of

Author contributions: G.L. and J.L. designed research; G.L., J.L., X.L., and T.Y. performed research; G.L. and T.Y. analyzed data; and G.L. and J.L. wrote the paper.

The authors declare no competing interest.

This article is a PNAS Direct Submission. V.R. is a guest editor invited by the Editorial Board.

[1]To whom correspondence may be addressed. Email: jing-li@pku.edu.cn.

This article contains supporting information online at https://www.pnas.org/lookup/suppl/doi:10.1073/pnas.2414241121/-/DCSupplemental.

Published November 18, 2024.

warmer North Atlantic in shaping hotter summer of Canada (18). Meanwhile, diminished Arctic sea ice concentration (SIC) has substantially impacted the regional climate of Canada, with the preceding decrease in sea ice in the Arctic being associated with intensified droughts and heatwaves during summer (17, 19). This teleconnection is maintained by wave-train structures, which are persistent from spring to summer. Previous studies have also identified the significant role of the positive phase of El Niño Southern Oscillation and Pacific Decadal Oscillation on intensifying Canadian fire activities of the following year by modulating the strength and position of western Canadian continental ridge (17). However, the extreme fire season in 2023 is unlikely to be related to the El Niño climate pattern because its effects are not expected to manifest in the summertime (20).

Having said the above, it is of great importance to investigate and clarify the key climate variability that drives the abnormal weather conditions and extreme fire events in Canada this year. In this study, we focus on ocean variability and identify the North Atlantic and Arctic as the major drivers of the abnormal summer 2023 climate conditions that favor the ignition and spread of wildfires in Canada. We have designed a comprehensive approach that includes multisource data analysis and climate model simulations to reveal the underlying mechanisms connecting this remote variability with Canadian fire weather. This research is of great importance for improving the fire near-term prediction ability and adaption and prevention ability to fire of the local government. We further anticipate that our findings will advance our knowledge about the variables influencing fire weather conditions in Canada, thereby improving wildfire modeling and forecasting efforts.

Results

Canadian Fire and Climate Anomalies in the Summer Season of 2023. Multiple fire proxy datasets, including the fire weather index (FWI) (21, 22), and satellite retrieved fire radiative power (FRP) (23), and fire count (FC) (23) were considered to comprehensively describe the intensity of fires in Canada. Specifically, FWI serves as a rating system that quantifies the atmospheric conditions conducive to fire ignition and spread taking meteorological elements into consideration (24). A higher FWI value suggests more favorable weather conditions for the occurrence of wildfires (25). FRP, FC, and BA products are indices assessing the intensity, occurrence number, and the spatial extent of fires (21, 26, 27), respectively.

Different fire proxies consistently show significant increases up to ~150% over Canada in summer 2023 compared to climatology (Fig. 1 *A*–*C*), especially over northern and northeastern parts. These areas, characterized by dense vegetation with high normalized difference vegetation index (NDVI), are susceptible to frequent ignition and fire propagation (28, 29). The FWI (Fig. 1*A*) exhibits the most notable positive anomaly, ranging from 1.5 to 2 times the climatological average. FC and FRP also both increased by 100 to 200%, with similar spatial distribution of the anomalies to that of FWI (Fig. 1 *B* and *C*).

The extreme burning emitted higher than normal smoke aerosols, including black carbon, organic carbon, and carbon monoxide (Fig. 1 *D*–*F*), analyzed by MERRA-2 reanalysis datasets. The distribution of these aerosol and gases are more uniform due to the atmospheric transport and mixing, with two major hotspots in western and eastern Canada respectively, but extends to eastern United States and north Atlantic. It is noted that the black carbon and organic carbon mass density applied in this study is throughout the atmospheric column and it captures the plumes for the Canadian fire peak events. Similar smoke transport patterns of this fire season are widely recognized in previous studies (30, 31). It is also noted that there are some differences between the distribution of pollutants and FWI distribution, as pollutants also depend on the content, type, and structure of combustibles (20).

Examination of climate variables further indicates that Canada experienced an abnormal weather condition that is conducive to fires. This includes the occurrence of higher than normal surface temperatures, reduced precipitation, local high-pressure systems, and intensified northward winds (Fig. 1 *G*–*I*), which promote fire

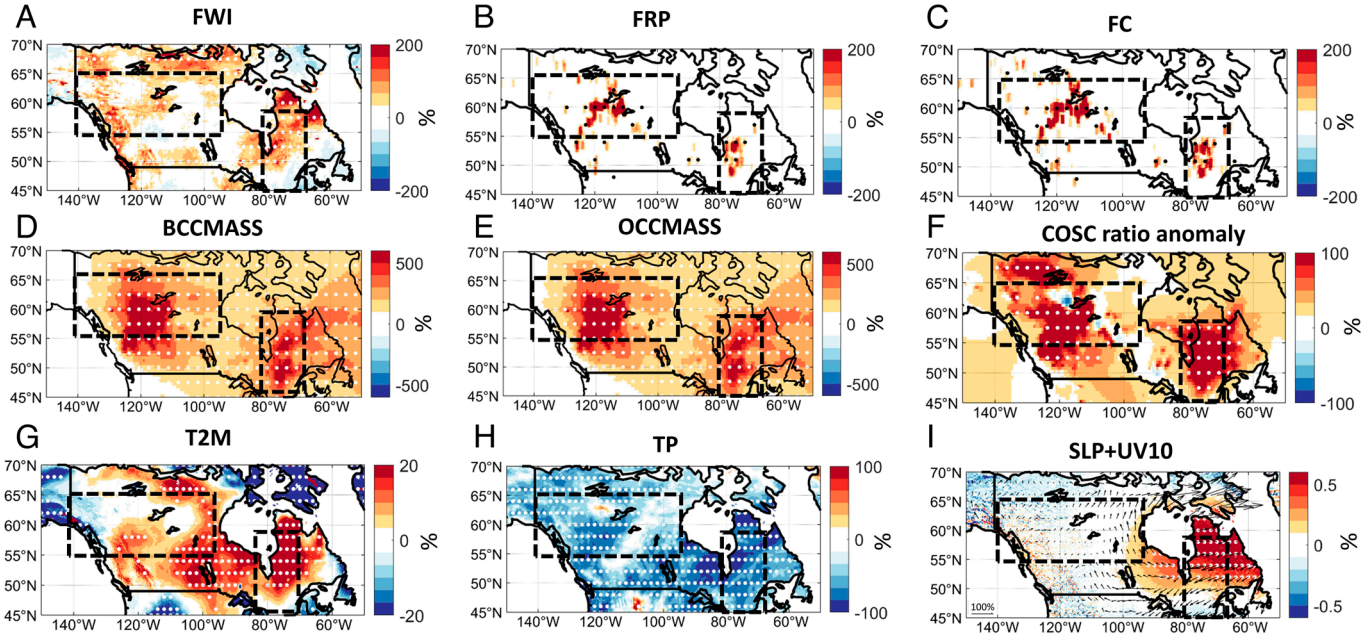

Fig. 1. Fire activity percentage anomaly in Canada in JJA in 2023 using multiple fire proxies, expressed as the ratio of the anomaly with respect to climatological mean calculated for the 1980-2019 period (2003-2020 period for FRP and FC due to the limited time span of satellite data). (*A*) FWI, (*B*) Fire radiative power (FRP), (*C*) FC, (*D*) BCCMASS density, (*E*) OCCMASS density, (*F*) COSC, (*G*) T2M, (*H*) Total precipitation (TP), and (*I*) Sea level pressure (SLP) + 10 m zonal and meridional wind (UV10) in JJA. The region containing white (black for FRP and FC) dots passes the Student's *t* test significance test with $P \leq 0.1$. The black dashed boxes correspond to main fire regions.

activity by reducing the moisture content of vegetation (fuels), increasing evaporation, and reducing vegetation transpiration (31). As a result, the exacerbation of these conditions not only amplifies the ignition of local fires but also facilitates the southward transportation of pollutants, thereby leading to adverse effects on ecology, human health, and the environment.

Teleconnection Linking Canadian Fire Weather with North Atlantic SST and Barents SIC. Considering the climatological peak season of fires and FWI in Canada (averaged between 140°W to 60°W and 50°N to 65°N) is the boreal summer (June, July, August, JJA), our main focus is on JJA fire activities (*SI Appendix*, Figs. S1 and S2). An examination using multiple reanalysis datasets reveals a robust correlation between JJA Canada FWI and JJA North Atlantic Sea Surface Temperature (SST) (30°N to 60°N, 60°W to 0°) as well as Barents SIC (SIC, defined as the area fraction) (72°N to 85°N, 0° to 70°E) in the leading months (May, June, and July, MJJ) (Fig. 2 *A* and *B* and *SI Appendix*, Figs. S3 *D–I* and S4 *D–I*). The delayed relationship between Barents SIC and Canada FWI can be attributed to the cumulative impact of the ice-albedo feedback and the duration required for atmospheric teleconnection, similar to the lagged relationship documented in the previous study (21). Positive changes in the North Atlantic are correlated with positive changes in the FWI in Eastern Canada, with a correlation as high as 0.6. On the other hand, decreases in Barents SIC are associated with positive anomalies in the FWI, particularly in central and northern Canada. Notably, the region with the most significant response is consistent with the fire anomaly and climatological range, further verifying the significant impact of SST and SIC on the 2023 fire event (Figs. 1 and 2 *A* and *B* and *SI Appendix*, Fig. S2). Because the correlation coefficient between detrended Barents SIC and North Atlantic SST is around −0.07 with a *P*-value of 0.62, these two variables can be considered independent, and thus their explained variances can be added. Historically, the combined variability of these two oceanic factors accounts for approximately 40% of the FWI variance (calculated by summing the squared correlation coefficients) across Canada on average, and over 60% in northwestern and eastern Canada (Fig. 2*C*). Similar correlation patterns are noted for FC and BA (*SI Appendix*, Fig. S5), confirming the teleconnection between Canadian fires and ocean variability, although the correlation patterns appear with a higher level of noise due to the inaccurate retrieval methods and limitations of clear-sky conditions in these two datasets (32, 33).

As correlation does not necessarily indicate causality, the physical relationship between Canadian fires and ocean variability is further verified through climate model simulations, i.e., Ocean Basin Experiments (OBEs; *Methods*). These simulations are carried out with the observed SST and SIC variability in the targeted ocean basin, while the SST and SIC in other ocean basins are maintained as seasonally varying climatology (*Methods*).

The response of the FWI to positive forcing of Atlantic SST is even stronger in the model simulations compared to the reanalysis

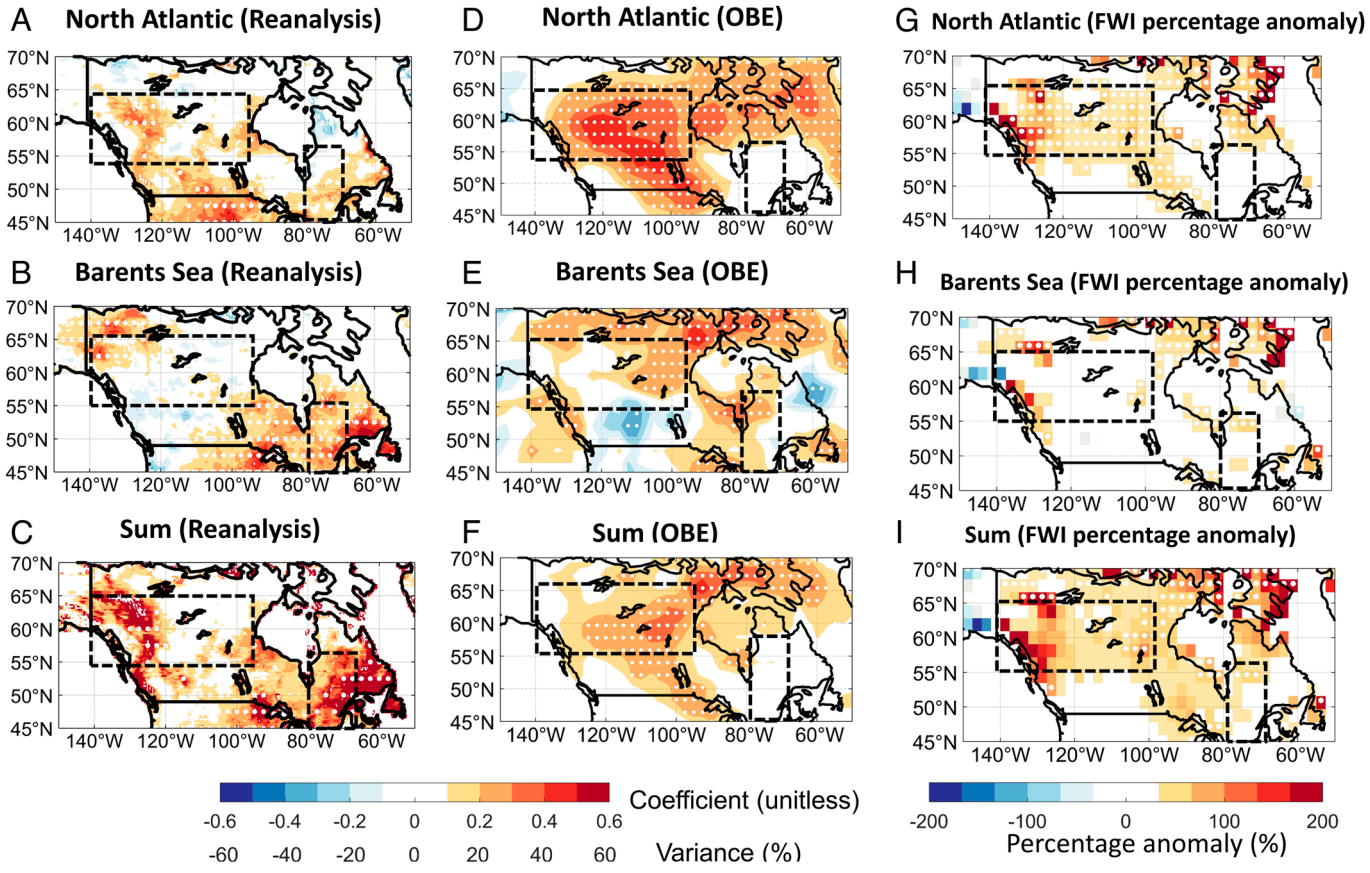

Fig. 2. Teleconnection pattern represented by correlation and explained variance between Canadian FWI and North Atlantic SST/Barents SIC variability with FWI percentage anomaly caused by North Atlantic SST/Barents SIC anomaly in 2023. (*A*) The distribution of correlation coefficients between JJA Canada FWI and JJA North Atlantic SST in ERA-5 reanalysis dataset. (*B*) Similar to (*A*), but for MJJ Barents SIC. (*C*) Total explained variance [calculated by the sum of squared correlation coefficients, that is $(a)^2 + (b)^2$] explained by North Atlantic SST and Barents SIC variability on FWI in the reanalysis dataset. (*D–F*) Similar to (*A–C*), but for the OBE. (*G*) FWI percentage anomaly caused by 2023 North Atlantic JJA SST anomaly calculated by OBE (*Methods*). (*H*) Similar to (*G*), but for MJJ Barents SIC. (*I*) Similar to g, but for the total FWI percentage anomaly of JJA North Atlantic SST and MJJ Barents SIC. The correlation coefficients in (*B*) and (*E*) are multiplied by −1 to indicate the Barents SIC reduction. Before the correlation coefficients are determined, all of the time series were detrended. The region containing white dots passes the Student's *t* test significance test with $P \leq 0.1$. The black dashed boxes correspond to main fire regions.

data. Significant positive anomalies extend throughout Canada, with the strongest signals in the central to western parts (Fig. 2 *A* and *D*). The reduced Barents SIC leads to significant increases in the FWI, particularly in central and northern Canada (Fig. 2*E*), which agrees qualitatively with the reanalysis results. The total variance of the FWI explained by the variability in the Atlantic and Barents Seas in the OBE reaches approximately 40% across most parts of Canada, highlighting the significant role of these two ocean basins in shaping Canadian weather and fire activities. In contrast, the FWI responses to other oceanic variabilities considered in the OBE are notably weak and insignificant (*SI Appendix*, Fig. S6 *A*–*E*), suggesting their negligible contribution to driving Canadian fire anomalies (*SI Appendix*, Fig. S6*F*).

We further focus on the 2023 summer burning season and examine the FWI responses to the observed Atlantic SST (JJA) and Barents SIC (MJJ). Remarkably, the geographic pattern of Atlantic SST and Barents SIC forced FWI anomalies coincides with the unprecedented wildfire anomaly witnessed during the 2023 burning season (Figs. 1*A*–*C* and 3*A*). This year also witnessed an unprecedentedly high JJA North Atlantic SST and anomalously low MJJ Barents SIC (Fig. 3 *B* and *C*). Global warming has also been identified as a driver of increased frequency, intensity, and duration of extreme wildfire events (34–36). For the specific event in 2023, global warming is unlikely to play the major role, since the great contributions of North Atlantic SST and Barents SIC are verified through detrended time series analysis and OBE simulations. Moreover, the Atlantic warming in summer 2023 is much higher than its linear trend, with SST anomalies close to 1 K, far higher than other years even after detrending (Fig. 3*E*). Similarly, Barents SIC reduction in this year is also much lower than its linear trend, with SIC anomalies around 10% (Fig. 3*F*). Therefore, the extreme fire event of this year should be mainly attributed to the abnormal Atlantic warming and the abnormally low Barents SIC, rather than general warming trend. It should also be noted that the entire North Atlantic is anomalously warm, especially in the northwestern part near Canada (Fig. 3*G*). Using the observed Atlantic SST and Barents SIC as the combined forcing field, the climate model simulated an increase in FWI of up to 100% in most parts of Canada (Fig. 2*I*). Simulations with individual forcing indicate that North Atlantic SST and Barents SIC result in 76% and 39% increases in FWI (Fig. 2 *G* and *H*), which account for approximately 52% and 27% of the observed 2023 FWI anomalies (Figs. 1*A* and 2 *G* and *H*), respectively. The simulated FWI anomaly pattern is also largely consistent with that observed (Figs. 1*A* and 2*I*), which highlights western and northern Canada as the main burning areas with hotspots. Overall, the FWI anomaly pattern simulated by the North Atlantic and Barents Sea forcings can together explain ~80% of the observed FWI anomalies throughout Canada (Figs. 1*A* and 2*I*). Because both the fire proxies and the ocean variability time series have undergone detrending, these correlations are robust and independent of the global warming background. Furthermore, there is no direct evidence to suggest that the 2023 fire was directly caused by global warming up to now (37, 38), and this topic is beyond the scope of this study and needs further investigation.

The above teleconnection between Canadian fire and ocean variability is realized through the modification of meteorological conditions by remote oceans, which is further examined here using reanalysis datasets, along with Atmospheric Model Intercomparison Project (AMIP) and OBE simulations. Both ERA-5 and OBE results indicate that warming anomalies in the North Atlantic correspond to higher temperatures (T2M, *SI Appendix*, Fig. S7 *A* and *B*), lower precipitation (TP, *SI Appendix*, Fig. S7 *B* and *F*), and a high-pressure system (SLP changes, *SI Appendix*, Fig. S7 *E* and *G*) over most parts of Canada, although a slight spatial shift is observed for simulated temperature changes. The pressure changes are further associated with stronger northerly winds, especially in the eastern part. Meanwhile, similar meteorological anomalies but with weaker magnitudes are observed for negative Barents SIC forcing (*SI Appendix*, Fig. S7 *I*–*K* and *M*–*O*). The North Atlantic SST and Barents SIC forced changes combined create hot and dry conditions in Canada that are prone to fires, with the stronger northerly winds promoting smoke transport to the United States. Indeed, the spatial pattern of FWI anomalies (*SI Appendix*,

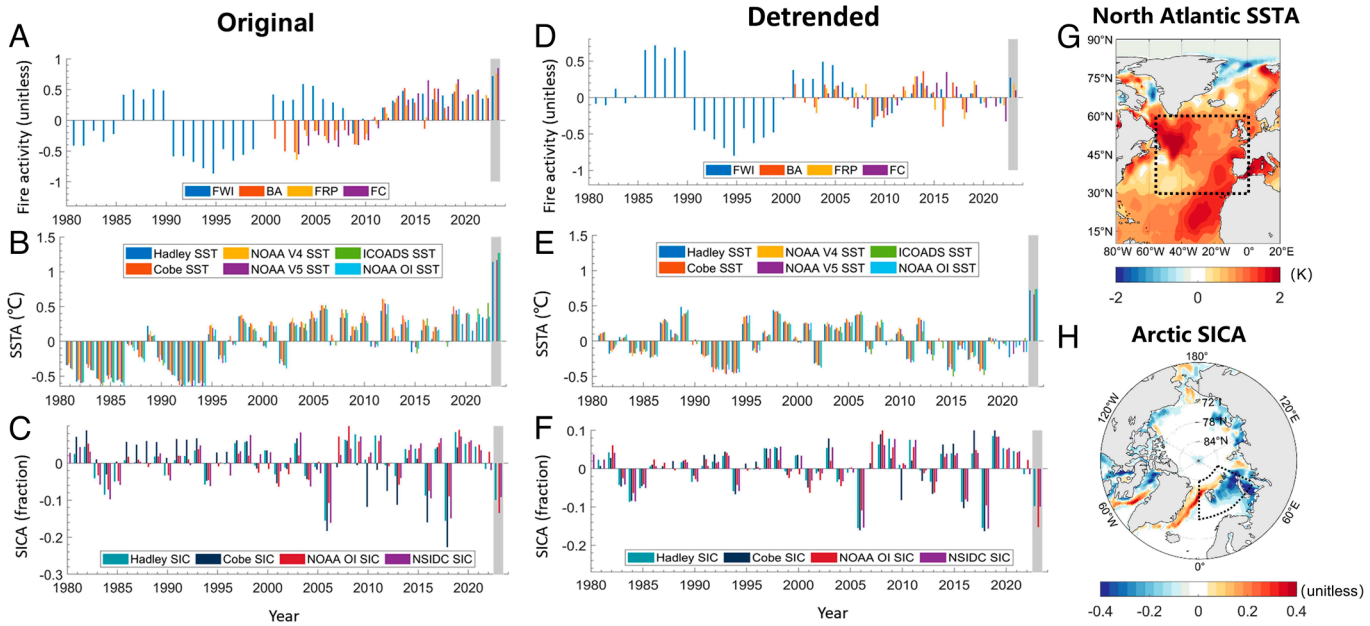

Fig. 3. (*A*–*F*) Annual mean of Canada fire activity proxies, North Atlantic SST, and Barents SIC. Bar charts of annual mean. (*A*) Standardized and 5-y moving average JJA fire activity proxies, (*B*) JJA North Atlantic SST anomaly (SSTA), and (*C*) MJJ Barents SIC anomaly (SICA) from 1980 to 2023 from different reanalysis datasets before detrending. (*D*–*E*) Similar to (*A*–*F*), but for the time series after detrending. FWI: FWI, BA: burned area, FRP: FRP, and FC: FC. The light gray rectangle represents the situation in 2023. (*G*) North Atlantic SST anomaly (SSTA) in JJA of 2023, and (*H*) Arctic SIC anomaly (SIC) in MJJ of 2023. The range of the black dashed box is the location of the North Atlantic in (*G*) and the Barents Sea in (*H*).

Fig. S7 *D*, *H*, *I*, and *P*) caused by the above meteorological changes estimated by the random forest model (*Methods*) agrees well with that of observation (Fig. 2 *A*, *B*, *D*, and *E*). The teleconnection patterns between Canadian meteorological variables, as well as FWI and North Atlantic SST/Barents SIC, are further supported by NCEP, MERRA-2 reanalysis datasets, and AMIP simulations (*SI Appendix*, Figs. S3 and S4).

In summary, a strong link has been identified between a teleconnection pattern that causes an increase in North Atlantic SST and/or a decrease in Barents SIC, and heightened wildfire activity in Canada. This teleconnection pattern modifies local weather conditions, leading to the extreme fire events. The combination of these two oceanic variations has the potential to account for up to 80% of the increased FWI in Canada during the summer of 2023, suggesting that they are the primary climate drivers behind this extreme event.

Physical Processes Underlying the Atlantic SST (Barents SIC)-Canadian Fire Teleconnection. In order to gain insights into the underlying mechanisms linking changes in North Atlantic SST and Barents SIC to fire weather in Canada, we examine the responses of atmospheric circulation patterns represented by the 500 hPa geopotential height (GPH500), 500 hPa zonal and meridional wind (U500 and V500), as well as vertical cross-sections of geopotential height (GPH) and vertical velocity in both reanalysis and OBE results (Fig. 4).

The elevated SST in the North Atlantic induces an increase in the temperature of the overlying air mass, leading to the formation of a local low-pressure system in the lower troposphere (Fig. 4 *A* and *B*). This atmospheric response triggers vertical uplift and divergence in the upper troposphere, resulting in high-pressure anomalies at 500 hPa (Fig. 4 *C* and *D*). The changes in surface pressure patterns then form an anomalous zonal circulation cell, which is distinguished by the presence of a high-pressure center at 500 hPa and descending motions from 200 hPa to near the surface above Canada (Fig. 4 *C* and *D*). Associated with this high-pressure center, north and northeast winds prevail on the southern side of the circulation cell (*SI Appendix*, Fig. S8 *C* and *G*). Meanwhile, the descending airflows undergo adiabatic heating, leading to increased temperature and dryness over most of Canada. The prevailing wind patterns also result in reduced moisture transport to Canada, exacerbating the arid conditions there and enhancing southward smoke transport.

On the other hand, the decrease in MJJ Barents SIC induces a pronounced warming effect in the Barents Sea, primarily driven by the ice-albedo feedback mechanism. This temperature increase, in turn, influences the thermal properties of the overlying atmosphere, leading to the formation of a localized low-pressure system in the upper troposphere (Fig. 4 *E* and *F*). The resulting signal acts as a source for the generation of Rossby waves and their subsequent propagation from west to east, manifested as a distinctive pattern of alternating high and low-pressure centers that arrive above Canada as an anomalous high pressure (Fig. 4 *E* and *F*). The presence of this high-pressure system corresponds to descending motions in the atmosphere, again creating drier and hotter air masses. Additionally, prevailing northerly winds on the western

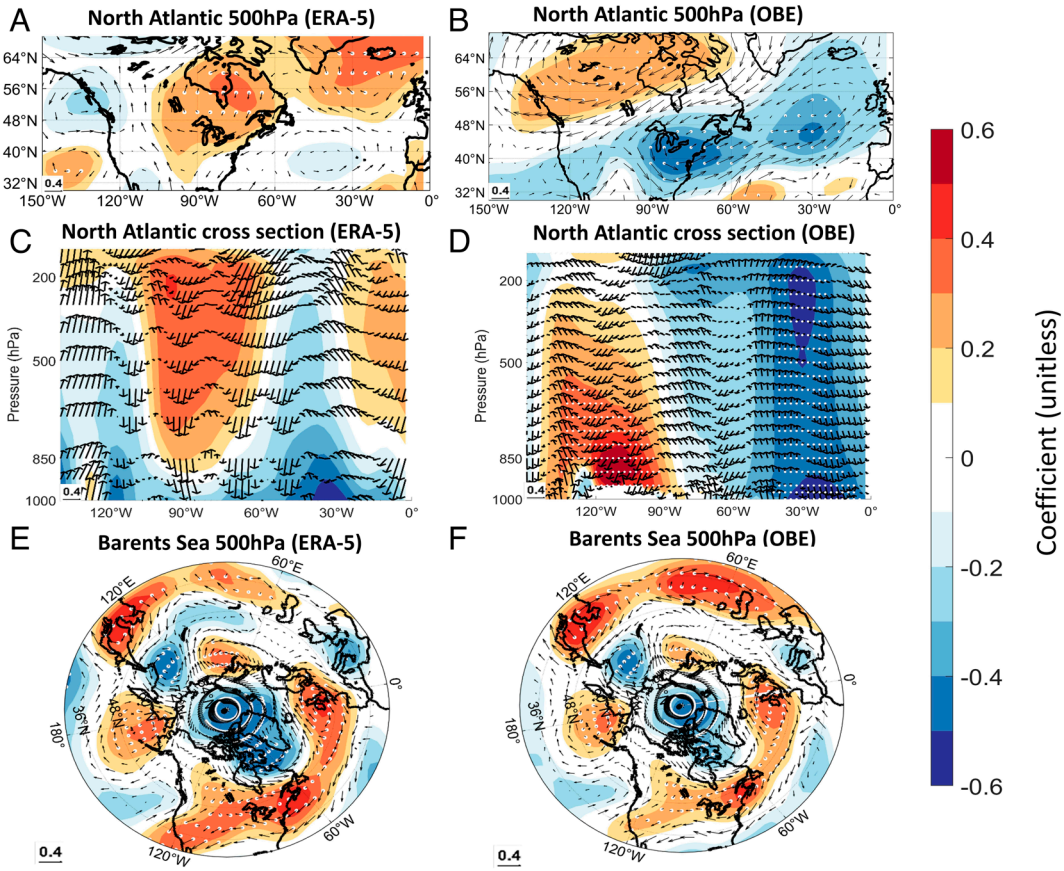

Fig. 4. Physical processes underlying the teleconnection. (*A*) The distribution of correlation coefficients between JJA 500 hPa GPH (shaded) +UV (arrows) and JJA North Atlantic SST in the ERA5 reanalysis (1980-2019). (*B*) similar to (*A*) but in OBE. (*C*) The cross-sections of correlation coefficients between zonal mean GPH (shaded), vertical and zonal wind (arrows) averaged from 40°N to 60°N and JJA North Atlantic SST in the ERA5 reanalysis (1980-2019). (*D*) similar to (*C*) but in OBE. (*E*) The distribution of correlation coefficients between JJA 500 hPa GPH (shaded) +UV (arrows) and MJJ Bering SIC in the (*E*) ERA5 reanalysis (1981-2020). (*F*) similar to (*E*) but in OBE. The correlation coefficients in (*E*) and (*F*) are multiplied by −1 to indicate the Barents SIC reduction. Before the correlation coefficients are determined, all of the time series were detrended. The region containing white dots passes the Student's *t* test significance test with $P \leq 0.1$.

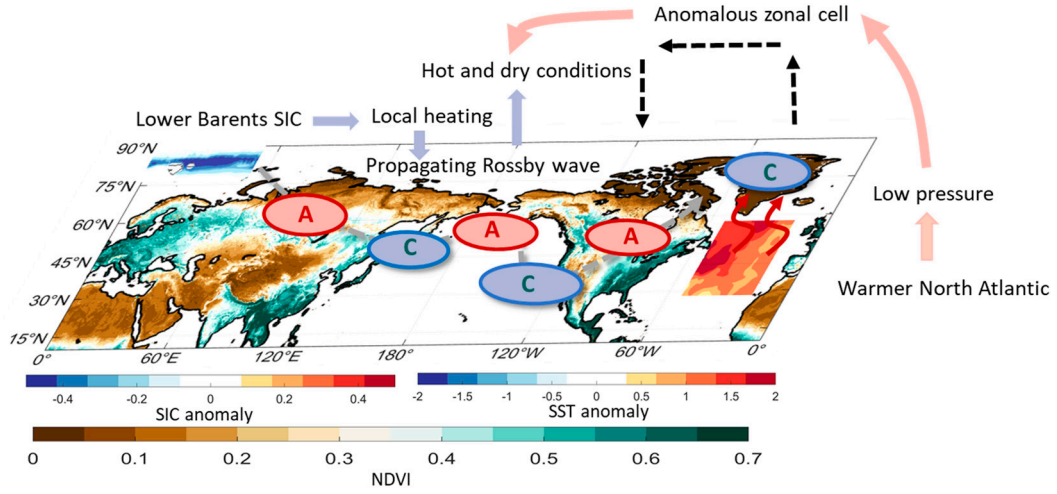

Fig. 5. Schematic illustration of the teleconnection mechanisms in a schematic diagram. Teleconnection between warmer North Atlantic SST (reduced Barents SIC) and more frequent fire activities in Canada. "A" and "C" represent anticyclonic and cyclonic circulations, respectively.

side of the anticyclone circulation, induced by the aforementioned high-pressure center, contribute to reduced moisture transport toward Canada. Notably, the location of this high-pressure center is different from that of the high-pressure system generated by the North Atlantic warming anomaly (Fig. 4 *A* and *B*), which could partially explain the different distribution of FWI anomalies in Canada under these two forcing fields (Fig. 2).

The above-mentioned physical processes are further validated by the relationship between Barents SIC and 500 hPa steam function in reanalysis datasets and the OBE (*SI Appendix*, Fig. S8). The Rossby wave propagation from the Barents Sea to Canada is supported by the correlation coefficients of the stream function (*SI Appendix*, Fig. S8). The reaction of the upper level stream function over Canada to the decreased SIC in the Barents Sea suggests the presence of a high-pressure center and descending airflow in this region. Since the wave propagation pathway travels a great distance and the initial conditions contain uncertainties and parameterizations, it is reasonable to expect that the model will not fully capture all the complex interactions and anomalies in the large-scale circulation. Still, there is a fair amount of agreement between the OBE's overall patterns and the reanalysis datasets.

In conclusion, the intricate physical mechanisms by which North Atlantic SST and Barents SIC influence the Canadian region have been succinctly captured within the outlined schematic diagram shown in Fig. 5. First, increased North Atlantic SST engenders the formation of a surface low-pressure system, which, in turn, leads to the establishment of a quasi-stationary high-pressure system akin to a blocking high over northern Canada. Reduced Barents SIC in the preceding month also forms a high-pressure system over Canada through propagating Rossby waves, mainly in eastern and southern Canada. The two systems collectively create hot and dry conditions and enhanced north and northwest winds, which favor the ignition, spread, and southward transport of wildfires.

Discussion

In summary, this study finds that increased SSTs in the North Atlantic and reduced SIC in the Barents Sea are the primary drivers of severe hot and dry weather in Canada during the summer of 2023. These factors contribute to about 80% of the Canadian FWI during this wildfire season. The study reveals that the Atlantic impacts Canadian weather by creating a regional circulation pattern with upward air motions over the Atlantic and downward motions over northern Canada. The teleconnection between Barents SIC and Canadian climate is established through Rossby waves, which travel around the high latitudes of the Northern Hemisphere and reach Canada as a high-pressure center, particularly in the southern part. These combined mechanisms lead to prolonged droughts, heatwaves, and increased northerly winds, creating favorable conditions for the generation and southward spread of wildfires. The findings of this study are robust and supported by various data analyses, including reanalysis datasets, AMIP simulations, and experiments using state-of-the-art climate models. Notably, unlike meteorological elements extending the long time period (1980-2019), the data of FC (2003-2020), FRP (2003-2020), and burned area (BA) (2001-2020) are only available during the satellite era. Nonetheless, the climate models are in good accordance with the observational analysis, mitigating the uncertainty associated with the relatively limited satellite records.

Previous studies have mostly focused on the increase in extreme events caused by global warming (13–15), while our research aims to reveal the specific variability and teleconnection mechanisms. In particular, compared with previous studies focusing on the 2023 catastrophic wildfire, this study highlights the significant contribution of SST and SIC variability to such extreme events. Previous studies have discussed the 2023 Canadian extreme fire event and related environmental issues (37, 38). Sáenz-Romero mentioned that the catastrophic forest fires in Canada has made Canadian forest a clear carbon source rather than a carbon sink, potentially contributing to global warming (37). Wang et al. focused on the impact of Canada's recording-breaking wildfires and discussed that the substantial amounts of greenhouse gases from forest and peat fires might contribute to the positive feedback to the climate, potentially further accelerating the global warming (38). However, up to now, these studies have no direct evidence to suggest that the 2023 fire was directly caused by global warming. Nonetheless, the contribution of North Atlantic SST and Barents SIC might be underestimated due to detrending data used in this study. Admittedly, both North Atlantic SST and Barents SIC changes may be related to global warming, as well as internal natural variability (39, 40). These two ocean basins might also be intrinsically connected, as North Atlantic SST variability could lead to the interannual and decadal variability of Arctic sea ice (41). These envision new challenges for discussing the impact and contribution of variability on wildfires, which will be thoroughly investigated in our future study.

Looking ahead, the vulnerable Canada region is poised to face even greater environmental challenges for two reasons. First, it is projected that Arctic SIC will continue to diminish until complete disappearance in September prior to the 2050s under the modest and extreme shared socioeconomic pathways (SSP2-4.5 and SSP5-8.5) (41). Even under the SSP1-2.6 scenario, the Arctic SIC might still be halved (41). Second, North Atlantic SST is expected to persistently rise due to the effects of global warming, despite of its warming hole and the slowdown of the AMOC (42, 43). The confluence of declining Arctic sea ice extent and warmer North Atlantic SST thus likely cause more frequent fire conditions in Canada according to the teleconnection revealed by this study. Furthermore, global warming and CO_2 fertilization have the potential to enhance vegetation growth, which in turn serves as fuel for wildfires. This warming trend also exacerbates warmer and drier conditions, characterized by exceptionally low water vapor deficit, thereby further amplifying the risk of wildfires in the mid to high latitudes (27, 44).

In essence, our investigation underscores that the projected reduction in Arctic sea ice and the warming of the North Atlantic are anticipated to contribute to an escalation in wildfires across Canada, making situations such as the summer of 2023 more likely to occur in the future, potentially accelerating the global warming trend. When combined with the exacerbating effects of global warming on wildfires, this compounded impact heightens the risk of devastating wildfires in Canada.

Methods

Fire Proxy Data. The current study uses the FWI, BA, FC, and FRP as monthly fire proxies as indicators of fire activity.

A grading system called the FWI uses variables including wind speed, surface temperature, TP, and surface pressure to determine how intense a fire is (22). It is composed of various components that consider the impact of fuel moisture and wind on wildfire behavior and propagation. A higher FWI indicates more favorable meteorological conditions for the occurrence of wildfires (25). This index is calculated by initial spread index and build-up index, and more frequently used for general public information about fire danger conditions in Canada (45–47). Daily FWI data (0.25° × 0.25°, 1981–2019) are sourced from the historical fire danger indices offering a straightforward way for quantifying the atmospheric conditions favorable for fire ignition and spread (21, 48). For additional analysis, the daily FWI is then averaged into monthly FWI.

Global data on total burned area at pixel and grid scales with 0.25° × 0.25° resolution are provided by BA products. We make use of the Copernicus Emergency Management Service's monthly BA product for the years 2001–2019 (26). Because Moderate Resolution Imaging Spectroradiometer (MODIS) fire products have a longer time span than more recent sensors like the Visible Infrared Imaging Radiometer Suite, FC and FRP datasets are derived from MODIS fire products. This product has significantly enhanced detection capabilities in boreal regions. For further analysis, monthly FC and FRP data from 2003 to 2019 are resampled to a monthly dataset after being interpolated to a 0.25° × 0.25° grid. We use data processing techniques for FC and FRP that are comparable to those used in earlier research (49).

Moreover, to demonstrate the impact of wildfires on air pollution in surrounding areas, we also used MERRA-2 monthly black carbon column mass density (BCCMASS), Organic carbon column mass density (OCCMASS), and monoxide surface concentration (COSC) (50, 51).

Meteorological Data. Because the FWI is largely determined by meteorological factors, such as wind speed, precipitation, and surface temperature (25), we mainly use monthly meteorological variables from the interpolated ERA5 reanalysis datasets to examine how these variables response to SST and SIC forcing in different ocean basins (52). Following Lawson and Armitage (25), we choose a spatial resolution of 0.25° × 0.25° for the following datasets: 10 m wind speed (WND10, computed from the meridional and zonal component of 10 m wind), SLP, TP, and 2 m temperature (T2M). The above-mentioned datasets span the time period from 1981 to 2019. We also use the corresponding variables from the MERRA-2 datasets (0.625° × 0.625°) and NCEP-NCAR Reanalysis 1 datasets (2.5° × 2.5°) to evaluate sensitivity to alternative reanalysis datasets (53, 54).

Furthermore, we utilize the following SST and ice datasets for the same period: International Comprehensive Ocean-Atmosphere Dataset (ICOADS SST, 2° × 2°), NOAA Optimum Interpolation SST version 2 (NOAA OI SST and SIC, 0.25° × 0.25°), Monthly Averaged Hadley Center Sea Ice and SST dataset (Hadley SST and SIC, 1° × 1°), Centennial in situ Observation-Based Estimates SST with SIC (COBE SST and SIC, 1° × 1°), National Oceanic and Atmospheric Administration Extended Reconstructed SST version 4 (NOAA V4 SST, 1° × 1°), NOAA Extended Reconstructed SST version 5 (NOAA V5 SST, 1° × 1°), and ICOADS (ICOADS SST, 2° × 2°) (55–57). Besides these reconstructed SST and SIC datasets, the more accurate SIC data provided by the National Snow and Ice Data Center from multiple satellite observations (NSIDC SIC) are also applied in this study (58).

Correlation and Contribution Analysis. To eliminate the impacts of global warming, all of the time series were detrended before calculating the correlation coefficients. Comparing the time series before and after detrending, it was found that the linear trend of global warming has a significant impact on fire proxies and SST, while its impact on SIC is relatively small (Fig. 3 *A*–*F*). Lag correlations are also conducted between JJA Canada FWI and North Atlantic SST as well as Barents SIC in seasons other than JJA (North Atlantic) and MJJ (Barents Sea), which indicate weaker correlation for the other seasons. Likewise, no similarly strong correlation is identified between JJA FWI and other parts of the Arctic. Therefore, the analysis in this study concentrates on JJA Canadian fire activity and JJA North Atlantic SST as well as MJJ Barents SIC.

Moreover, based on the OBE results and observed SST and SIC in 2023, we can calculate the FWI anomaly ($\mathrm{FWI}_{\mathrm{ano}}$) associated with the SST and SIC anomalies in 2023. The specific calculation method is summarized in Eq. **1** and described as follows. First, the meteorological variables simulated by the OBE are passed through the random forest regression (RFR) model (described below) to obtain the corresponding FWI. Second, a regression analysis is conducted between the FWI and the SST (SIC). Finally, the regression coefficients are scaled by the observed JJA North Atlantic SST and MJJ Bering SIC anomalies in 2023:

$$\mathrm{FWI}_{\mathrm{ano}} = \mathrm{reg}(\mathrm{OBE\ \ FWI}, \mathrm{SST(SIC)}) \times \mathrm{SST(SIC)}_{\mathrm{ano},2023}, \qquad [1]$$

where $\mathrm{FWI}_{\mathrm{ano}}$ is the FWI anomalies associated with observed SST and SIC anomalies in 2023, $\mathrm{reg}(\mathrm{OBE\ \ FWI}, \mathrm{SST(SIC)})$ is the regression coefficient of FWI against SST(SIC), and $\mathrm{SST(SIC)}_{\mathrm{ano},2023}$ is the JJA North Atlantic SST and MJJ Bering SIC anomalies in 2023.

Furthermore, by applying $\mathrm{FWI}_{\mathrm{ano}}$ and Eq. **2**, we calculated the contributions of North Atlantic SST and Barents SIC anomalies to the Canadian FWI anomaly of summer 2023.

$$\mathrm{Contribution}_{\mathrm{force}} = \frac{\mathrm{FWI}_{\mathrm{ano}}}{\mathrm{FWI}_{\mathrm{ano},2023}} \times 100\,\%, \qquad [2]$$

where $\mathrm{Contribution}_{\mathrm{force}}$ is the contribution of SST and SIC forcing to Canadian FWI anomaly of summer 2023, $\mathrm{FWI}_{\mathrm{ano},2023}$ is the observed FWI anomalies of summer 2023.

Furthermore, considering that the correlation coefficient between detrended Barents SIC and North Atlantic SST is approximately −0.07 with a *P*-value of 0.62, these two variables are independent. Consequently, their explained variances can be combined as the total explained variances of these two factors.

Climate Model Simulations. We carried out a series of forcing experiments using the Community Earth System Model-Community Atmosphere Model version 5 (CESM-CAM5), in order to examine the underlying mechanism by which North Atlantic SST and Arctic SIC affect Canada (*SI Appendix*, Fig. S9) (59). The decision was made in order to capitalize on CAM5's improved capabilities, specifically its increased ability to simulate physical processes and climate dynamics at high latitudes compared with the previous model version (Community Atmosphere Model version 4) (60).

To isolate the meteorological response in Canada to this remote forcing, the model was updated to include the SST and SIC variability from 1979 to 2019 based on observed SST and SIC utilizing data from the Hadley SST and SIC datasets. Specifically, in North Atlantic OBE, North Atlantic SST (30°N to 60°N, 60°W to 0°) was

updated with observed SST variability. Similarly, in Arctic OBE, Barents SIC (78°N to 85°N, 0° to 60°E) was updated with observed SIC variability. Meanwhile, SST and SIC in the other ocean basins remain as seasonally varying climatology (*SI Appendix*, Fig. S9). In order to identify the distinct roles of the North Atlantic and Arctic, we also assessed the impact of other ocean basins. In particular, the tropical Atlantic (20°N to 20°S), tropical Pacific (20°N to 20°S), tropical Indian (20°N to 20°S), North Pacific (25°N to 75°N), and Southern Ocean (60°S to 80°S) regions were individually added to the monthly SST variability utilizing data from the Hadley SST and SIC datasets, with a buffer zone of 10° added to the north and south of the forcing region, whereas the other ocean basins remain in climatological state. These simulations are referred to as OBEs hereafter and in the main text. An eight-member ensemble simulation with different starting conditions was conducted. The ensemble mean was applied in the further research. Specifically, we first ran a CAM simulation with climatological forcing for eight model years, and the eight members of the ensemble then began with the restart files for each year. Next, we conducted benchmark experiments based on climatological mean SST and SIC. The responses of the atmosphere to SST (SIC) forcing are calculated as the difference between OBE forced by observed SST and SIC and the benchmark simulation results. This simulation is similar to that used in earlier research (61). It is noted that these are atmosphere-only experiments.

AMIP Experiments. Meteorological conditions from the AMIP experiments support the reanalysis data. The atmospheric models used in these simulations are compelled by observed SIC and SST (62). The meteorological variables for 13 models are accessible in AMIP, each of which includes several ensemble members (63). Details on the chosen models are given in *SI Appendix*, Table S1. The response of meteorological variables in Canada to North Atlantic SST and Arctic SIC since the 1980s is examined using data spanning from 1980 to 2014. For use in later analyses, all of the afore-mentioned datasets in the CMIP6 have been interpolated to a 1° × 1° resolution.

The RFR Model. While daily meteorological variables like T2M, relative humidity, TP, and WND10 can be explicitly used to calculate the FWI (64), the limited availability of outputs from the OBE and AMIP results makes it difficult to calculate the FWI using the standard formulas. Thus, we use a RFR method to estimate FWI in the OBE and AMIP results (61, 65, 66). The relative importance of each input variable is evaluated using Gini importance, which is a metric that is defined as the total average decrease in node impurity over the whole ensemble tree collection. In sum, the predictors are boreal spring T2M, SLP, TP, and WND10, and the predicted variable is FWI, a direct matrix for measuring fire weather potential.

To minimize prediction errors caused by varying initial values and weights, the 200-tree RFR model is trained 200 times. The model's performance is evaluated and adjusted using fivefold cross-validation. The average correlation coefficient between the observed and predicted values is 0.86, which surpasses the significance level of $P \leq 0.01$ according to the Student's t test.

Data, Materials, and Software Availability. The Normalized Vegetation Difference Vegetation Index (NDVI) dataset was downloaded from NASA ARC ECOCAST GIMMS NDVI3g v1p0 NDVI (67). All other data are included in the manuscript and/or *SI Appendix*.

ACKNOWLEDGMENTS. We thank the editor and anonymous reviewers, who helped improve the manuscript substantially. This study is funded by the National Natural Science Foundation of China Grant Nos. 42425503 and 42175144.

Author affiliations: [a]Department of Atmospheric and Oceanic Sciences, School of Physics, Peking University, Beijing 100871, China; and [b]Institute of Atmospheric Physics, Chinese Academy of Sciences, Beijing 100029, China

1. D. Bowman *et al.*, Fire in the Earth system. *Science* **324**, 481–484 (2009).
2. C. C. Hanes *et al.*, Fire-regime changes in Canada over the last half century. *Can. J. For. Res.* **49**, 256–269 (2019).
3. B. J. Stocks *et al.*, Large forest fires in Canada, 1959–1997. *J. Geophys. Res. Atmos.* **108**, 8149 (2002).
4. C. A. Kolden, J. T. Abatzoglou, M. W. Jones, P. Jain, Wildfires in 2023. *Nat. Rev. Earth Environ.* **5**, 238–240 (2024).
5. Z. Wang *et al.*, Severe global environmental issues caused by canada's record-breaking wildfires in 2023. *Adv. Atmos. Sci.* **41**, 565–571 (2024).
6. P. Jain, X. L. Wang, M. D. Flannigan, Trend analysis of fire season length and extreme fire weather in North America between 1979 and 2015. *Int. J. Wildland Fire* **26**, 1009–1020 (2017).
7. M. C. Kirchmeier-Young, F. W. Zwiers, N. P. Gillett, A. J. Cannon, Attributing extreme fire risk in Western Canada to human emissions. *Clim. Change* **144**, 365–379 (2017).
8. M. A. Parisien *et al.*, Abrupt, climate-induced increase in wildfires in British Columbia since the mid-2000s. *Commun. Earth Environ.* **4**, 309 (2023).
9. J. T. Abatzoglou, A. P. Williams, Impact of anthropogenic climate change on wildfire across western US forests. *Proc. Natl. Acad. Sci. U.S.A.* **113**, 11770–11775 (2016).
10. S. C. P. Coogan, F.-N. Robinne, P. Jain, M. D. Flannigan, Scientists' warning on wildfire–A Canadian perspective. *Can. J. For. Res.* **49**, 1015–1023 (2019).
11. M. Flannigan, B. Stocks, M. Turetsky, M. Wotton, Impacts of climate change on fire activity and fire management in the circumboreal forest. *Global Change Biol.* **15**, 549–560 (2009).
12. J. F. Xiao, Q. L. Zhuang, Drought effects on large fire activity in Canadian and Alaskan forests. *Environ. Res. Lett.* **2**, 044003 (2007).
13. W. J. Cai *et al.*, Increasing frequency of extreme El Nino events due to greenhouse warming. *Nat. Clim. Change* **4**, 111–116 (2014).
14. E. M. Fischer, R. Knutti, Anthropogenic contribution to global occurrence of heavy-precipitation and high-temperature extremes. *Nat. Clim. Change* **5**, 560–564 (2015).
15. A. D. King, D. J. Karoly, B. J. Henley, Australian climate extremes at 1.5 °C and 2 °C of global warming. *Nat. Clim. Change* **7**, 412 (2017).
16. B. Mohamed, F. Nilsen, R. Skogseth, Interannual and decadal variability of sea surface temperature and sea ice concentration in the barents sea. *Remote Sens.* **14**, 4413 (2022).
17. R. E. Petrie, L. C. Shaffrey, R. T. Sutton, Atmospheric response in summer linked to recent Arctic sea ice loss. *Q. J. R. Meteorol. Soc.* **141**, 2070–2076 (2015).
18. A. Shabbar, W. Skinner, Summer drought patterns in Canada and the relationship to global sea surface temperatures. *J. Clim.* **17**, 2866–2880 (2004).
19. M. R. Song, J. P. Liu, C. Y. Wang, Spring Arctic sea ice as an indicator of North American summer rainfall. *Int. J. Climatol.* **32**, 1354–1361 (2012).
20. B. Owens, Why are the canadian wildfires so bad this year? *Nature* **618**, 439–440 (2023).
21. A. Carvalho, M. D. Flannigan, K. Logan, A. I. Miranda, C. Borrego, Fire activity in Portugal and its relationship to weather and the Canadian fire weather index system. *Int. J. Wildland Fire* **17**, 328–338 (2008).
22. Copernicus Climate Change Service, Climate Data Store, Fire danger indices historical data from the Copernicus Emergency Management Service. Copernicus Climate Change Service (C3S) Climate Data Store (CDS). https://doi.org/10.24381/cds.0e89c522. Accessed 16 December 2023.
23. J. W. Kaiser *et al.*, Biomass burning emissions estimated with a global fire assimilation system based on observed fire radiative power. *Biogeosciences* **9**, 527–554 (2012).
24. A. P. Dimitrakopoulos, A. M. Bemmerzouk, I. D. Mitsopoulos, Evaluation of the Canadian fire weather index system in an eastern Mediterranean environment. *Meteorol. Appl.* **18**, 83–93 (2011).
25. B. D. Lawson, O. B. Armitage, *Weather Guide for the Canadian Forest Fire Danger Rating System* (Canadian Forest Service, Northern Forestry Center, 2008), pp. 1–84.
26. Copernicus Climate Change Service, Climate Data Store, Fire burned area from 2001 to present derived from satellite observation. Copernicus Climate Change Service (C3S) Climate Data Store (CDS). https://doi.org/10.24381/cds.f333cf85. Accessed 13 December 2023.
27. J. G. Canadell *et al.*, Multi-decadal increase of forest burned area in Australia is linked to climate change. *Nat. Commun.* **12**, 6921 (2021).
28. J. C. Ju, J. G. Masek, The vegetation greenness trend in Canada and US Alaska from 1984–2012 Landsat data. *Remote Sens. Environ.* **176**, 1–16 (2016).
29. C. C. Simpson, H. G. Pearce, A. P. Sturman, P. Zawar-Reza, Behaviour of fire weather indices in the 2009–10 New Zealand wildland fire season. *Int. J. Wildland Fire* **23**, 1147–1164 (2014).
30. C. S. Eastaugh, H. Hasenauer, Deriving forest fire ignition risk with biogeochemical process modelling. *Environ. Model. Softw.* **55**, 132–142 (2014).
31. S. L. Goodrick, G. L. Achtemeier, N. K. Larkin, Y. Q. Liu, T. M. Strand, Modelling smoke transport from wildland fires: A review. *Int. J. Wildland Fire* **22**, 83–94 (2013).
32. J. Brennan, J. L. Gómez-Dans, M. Disney, P. Lewis, Theoretical uncertainties for global satellite-derived burned area estimates. *Biogeosciences* **16**, 3147–3164 (2019).
33. J. X. Chen *et al.*, Overview of the performance of satellite fire products in China: Uncertainties and challenges. *Atmos. Environ.* **268**, 118838 (2022).
34. P. T. Brown *et al.*, Climate warming increases extreme daily wildfire growth risk in California. *Nature* **621**, 760 (2023).
35. J. D. Coop, S. A. Parks, C. S. Stevens-Rumann, S. M. Ritter, C. M. Hoffman, Extreme fire spread events and area burned under recent and future climate in the western USA. *Global Ecol. Biogeogr.* **31**, 1949–1959 (2022).
36. S. El Garroussi, F. Di Giuseppe, C. Barnard, F. Wetterhall, Europe faces up to tenfold increase in extreme fires in a warming climate. *NPJ Clim. Atmos. Sci.* **7**, 30 (2024).
37. C. Sáenz-Romero, Arriving at a tipping point for worldwide forest decline due to accelerating climatic change. *For. Chron.* **100**, 5–7 (2024).
38. Z. Wang *et al.*, Severe global environmental issues caused by Canada's record-breaking wildfires in 2023. *Adv. Atmos. Sci.* **41**, 565–571 (2024).
39. R. Hand, N. S. Keenlyside, N. E. Omrani, J. Bader, R. J. Greatbatch, The role of local sea surface temperature pattern changes in shaping climate change in the North Atlantic sector. *Clim. Dynam.* **52**, 417–438 (2019).
40. L. H. Smedsrud *et al.*, The role of the barents sea in the arctic climate system. *Rev. Geophys.* **51**, 415–449 (2013).
41. D. Notz *et al.*, Arctic Sea Ice in CMIP6. *Geophys. Res. Lett.* **47**, e2019GL086749 (2020).
42. W. Liu, A. V. Fedorov, S.-P. Xie, S. Hu, Climate impacts of a weakened Atlantic meridional overturning circulation in a warming climate. *Sci. Adv.* **6**, eaaz4876 (2020).
43. H. M. Sung *et al.*, Future changes in the global and regional sea level rise and sea surface temperature based on CMIP6 Models. *Atmosphere* **12**, 90 (2021).
44. B. Zheng *et al.*, Record-high CO_2 emissions from boreal fires in 2021. *Science* **379**, 912–917 (2023).
45. B. D. Amiro *et al.*, Fire weather index system components for large fires in the Canadian boreal forest. *Int. J. Wildland Fire* **13**, 391–400 (2004).
46. B. J. Stocks *et al.*, Canadian forest fire danger rating system–An overview. *For. Chron.* **65**, 258–265 (1989).
47. X. L. Wang *et al.*, Critical fire weather conditions during active fire spread days in Canada. *Sci. Total Environ.* **869**, 161831 (2023).

48. H. Zheng *et al.*, ENSO-related fire weather changes in Southeast and equatorial Asia: A quantitative evaluation using fire weather index. *J. Geophys. Res. Atmos.* **128**, e2023JD039688 (2023).
49. G. Y. Liu *et al.*, Increasing fire weather potential over Northeast China linked to declining bering sea ice. *Geophys. Res. Lett.* **50**, e2023GL105931 (2023).
50. Global Modeling and Assimilation Office (GMAO), MERRA-2 tavgM_2d_slv_Nx: 2d, Monthly mean, Time-Averaged, Single-Level, Assimilation, Single-Level Diagnostics V5.12.4, Greenbelt, MD, USA. Goddard Earth Sciences Data and Information Services Center (GES DISC). https://doi.org/10.5067/AP1B0BA5PD2K. Accessed 26 December 2023.
51. Global Modeling and Assimilation Office (GMAO). MERRA-2 tavgU_2d_chm_Nx: 2d, diurnal, Time-Averaged, Single-Level, Assimilation, Carbon Monoxide and Ozone Diagnostics V5.12.4, Greenbelt, MD, USA. Goddard Earth Sciences Data and Information Services Center (GES DISC). https://doi.org/10.5067/5KFZ6GXRHZKN. Accessed 26 December 2023.
52. H. Hersbach *et al.*, ERA5 monthly averaged data on single levels from 1940 to present. Copernicus Climate Change Service (C3S) Climate Data Store (CDS). https://doi.org/10.5067/5KFZ6GXRHZKN. Accessed 17 December 2023.
53. Global Modeling and Assimilation Office (GMAO). MERRA-2 tavgM_2d_flx_Nx: 2d, Monthly mean, Time-Averaged, Single-Level, Assimilation, Surface Flux Diagnostics V5.12.4, Greenbelt, MD, USA, Goddard Earth Sciences Data and Information Services Center (GES DISC). https://doi.org/10.5067/5KFZ6GXRHZKN. Accessed 26 December 2023.
54. E. Kalnay *et al.*, The NCEP/NCAR 40-year reanalysis project. *Bull. Am. Meteorol. Soc.* **77**, 437–471 (1996).
55. B. Y. Huang *et al.*, Extended reconstructed sea surface temperature version 4 (ERSST.v4). Part I: Upgrades and intercomparisons. *J. Clim.* **28**, 911–930 (2015).
56. B. Y. Huang *et al.*, Improvements of the daily optimum interpolation sea surface temperature (DOISST) version 2.1. *J. Clim.* **34**, 2923–2939 (2021).
57. N. A. Rayner *et al.*, Global analyses of sea surface temperature, sea ice, and night marine air temperature since the late nineteenth century. *J. Geophys. Res. Atmos.* **108**, 4407 (2003).
58. N. DiGirolamo *et al.*, Sea Ice Concentrations from Nimbus-7 SMMR and DMSP SSM/I-SSMIS Passive Microwave Data. (NSIDC-0051, Version 2). Boulder, Colorado USA. NASA National Snow and Ice Data Center Distributed Active Archive Center. https://doi.org/10.5067/MPYG15WAA4WX. Accessed 8 January 2024.
59. H. Yu *et al.*, Interannual variability and trends of combustion aerosol and dust in major continental outflows revealed by MODIS retrievals and CAM5 simulations during 2003–2017. *Atmos. Chem. Phys.* **20**, 139–161 (2020).
60. S. Y. Zhang, G. Zeng, X. Y. Yang, V. Iyakaremye, Z. X. Hao, Connection between interannual variation of spring precipitation in Northeast China and preceding winter sea ice over the Barents Sea. *Int. J. Climatol.* **42**, 1922–1936 (2022).
61. G. Y. Liu, J. Li, Z. J. Jiang, X. C. Li, Impact of sea surface temperature variability at different ocean basins on dust activities in the gobi desert and North China. *Geophys. Res. Lett.* **49**, e99821 (2022).
62. D. Ackerley, R. Chadwick, D. Dommenget, P. Petrelli, An ensemble of AMIP simulations with prescribed land surface temperatures. *Geosci. Model Develop.* **11**, 3865–3881 (2018).
63. V. Eyring *et al.*, Overview of the coupled model intercomparison project phase 6 (CMIP6) experimental design and organization. *Geosci. Model Develop.* **9**, 1937–1958 (2016).
64. J. D. Young, A. E. Thode, C. H. Huang, A. A. Ager, P. Z. Fulé, Strategic application of wildland fire suppression in the southwestern United States. *J. Environ. Manage.* **245**, 504–518 (2019).
65. G. Liu, J. Li, T. Ying, Amundsen sea ice loss contributes to Australian wildfires. *Environ. Sci. Technol.* **58**, 6716–6724 (2024).
66. G. Y. Liu, J. Li, T. Ying, The shift of decadal trend in Middle East dust activities attributed to North Tropical Atlantic variability. *Sci. Bull.* **68**, 1439–1446 (2023).
67. J. Pinzon, C. Tucker., A non-stationary 1981–2012 AVHRR NDVI3g time series. NDVI from NASA ARC ECOCAST GIMMS NDVI3g v1p0: Version 1.0. https://iridl.ldeo.columbia.edu/SOURCES/.NASA/.ARC/.ECOCAST/.GIMMS/.NDVI3g/.v1p0/.ndvi/index.html#info. Accessed 20 September 2023.